# scientific reports



# **OPEN**

# Numerical simulation and experimental study of suspended particulate matter removal for efficient water recovery and reuse in solid-liquid separation

Manikprabhu Dhanorkar¹, Ishan Mishra², Rohan Sawant², Kamal Sharma³, Chandrakant Sonawane²,8⊠, Md Irfanual Haque Siddiqui⁴, Intesaaf Ashraf⁵ & Ghanshyam G. Tejani<sup>6,7</sup>

In the present study, an empirical investigation was undertaken to evaluate the efficacy of a hydrocyclone in separation processes, followed by its implementation within a biogas plant setting. The laboratory phase employed sawdust as a surrogate material to facilitate hydrocyclone testing, while biogas slurry served as the practical material for subsequent experimentation within the biogas plant. The separation efficiency was approximately 50% for particles in the 50–200-micron range. Computational Fluid Dynamics (CFD) simulations were performed using the Fluent module embedded within ANSYS, employing the Renormalization Group (RNG) k –  $\epsilon$  turbulence model to numerically solve the three-dimensional Navier–Stokes equations, thereby facilitating precise predictions of swirl-induced phenomena. However, a notable disparity between the numerical results and experimental data was observed. Further refinement and calibration of the numerical model are required to align it more closely with the acquired experimental insights. In conclusion, the study suggests that approximately 40% of wastewater can be reclaimed and reused using the evaluated method. The overall study demonstrates the potential of the hydrocyclone to improve the efficiency of separation processes within a biogas plant setting.

**Keywords** Biogas plant, Hydrocyclones, Anaerobic digester, CFD, Experimental study

Solid-waste management is a global challenge that demands sustainable solutions. Biogas technology has emerged as an effective tool for managing organic wet waste. In India, millions of domestic biogas plants have been installed, and large-scale plants with capacities ranging from 5 to 500 tons per day now process municipal solid waste. These plants primarily produce biogas and digestate (spent slurry). While biogas is widely utilized, digestate has high manure potential and remains underexplored for solid and liquid manure production. The biomethanation process uses equal amounts of water and organic waste, resulting in twice the volume of digestate as input waste. Small-scale plants often ignore wastewater reuse, while large facilities face challenges in managing digestate due to its high suspended solid content (8–10%) and complex composition. Presently, digestate is typically drained without treatment, representing a significant waste of resources. No existing technology can efficiently separate solids and liquids in digestate while reclaiming water and solids for reuse. Biogas production has grown significantly in the twenty-first century, offering a sustainable alternative to conventional fuels due to its low carbon emissions, ease of production, and adaptability. Anaerobic digesters (AD) hold untapped energy potential, particularly in Europe, where agricultural byproducts and organic waste are key feedstocks<sup>2</sup>.

<sup>1</sup>Symbiosis Centre for Waste Resource Management, Symbiosis International (Deemed University), Pune, India. <sup>2</sup>Symbiosis Institute of Technology, Symbiosis International (Deemed University), Pune, India. <sup>3</sup>Department of Mechanical Engineering, GLA University, Mathura, India. <sup>4</sup>Department of Mechanical Engineering, College of Engineering, King Saud University, Riyadh 12372, Saudi Arabia. <sup>5</sup>Department of Mechanical Engineering, UCL, London, UK. <sup>6</sup>Department of Industrial Engineering and Management, Yuan Ze University, ., Taiwan. <sup>7</sup>Applied Science Research Center, Applied Science Private University, 11937, Amman, Jordan. <sup>8</sup> Symbiosis Center for Nanoscience and Nanotechnology, Symbiosis International (Deemed University), Pune, India. <sup>Me</sup>email: crsonawane@gmail.com

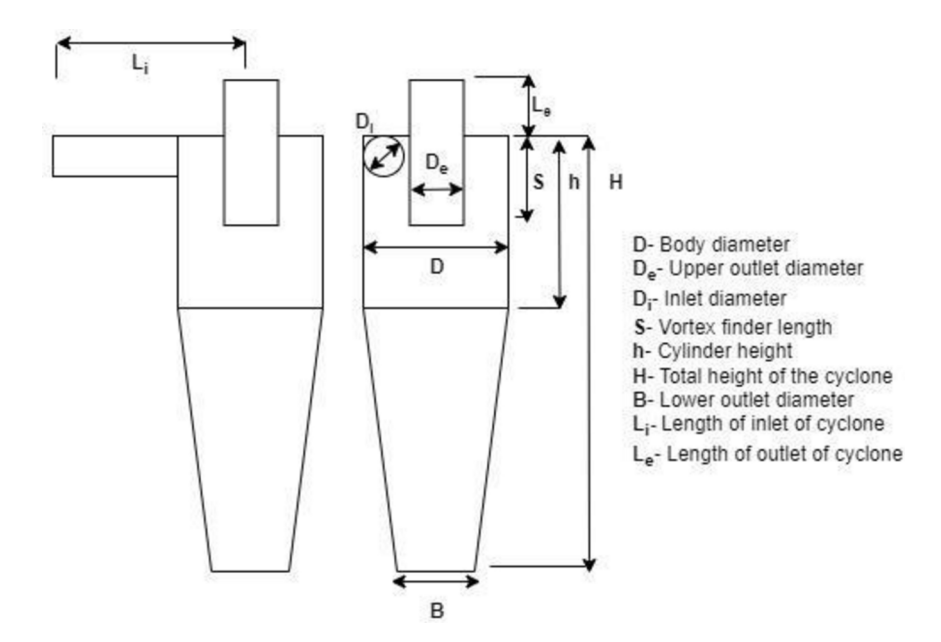


Fig.. 1. Design parameters.

Ratios	D <sub>i</sub> /D	D <sub>e</sub> /D	H/D	h/D	S/D	B/D	L <sub>i</sub> /D	L <sub>e</sub> /D
Current model	0.212	0.2125	2.2083	0.625	0.5	0.212	0.833	0.416

**Table 1**. Dimensional Ratios for Hydrocyclone Design: Optimized Proportions for Enhanced Separation Efficiency.

Sr No	Parameter	Base Design (mm)	Sr No	Parameter	Base Design (mm)	Sr No	Parameter	Base Design (mm)
1	D	240	4	S	120	7	В	51
2	Di	51	5	Н	150	8	L	200
3	De	51	6	Н	530	9	L <sub>e</sub>	100

**Table 2**. Physical Dimensions of the Hydrocyclone Based on the Selected Dimensional Ratios.

In India, biogas technology addresses waste management challenges, especially in urban and rural areas, where food waste has high biomethane production potential<sup>3</sup>. Various methods for separating nutrients from biogas slurry include sieving, screw presses, centrifugation, ultrafiltration, and sedimentation<sup>2,6-8</sup>. Hydrocyclones are promising devices for separating solid waste from liquids, particularly particles in the 1-10-micron range. They are widely used in waste management and bio waste treatment plants<sup>9</sup>. Studies<sup>4,5</sup> have demonstrated their effectiveness in separating fine particles such as plastics, sand, and organic matter from wastewater<sup>10–13</sup>. However, most of these studies focus on specific applications, and limited research addresses hydrocyclones' use in biogas plants for digestate separation. This study addresses the gap by experimentally and numerically evaluating a hydrocyclone's separation potential in a biogas plant setting. Laboratory tests were conducted using sawdust as a surrogate material, followed by real-world testing with biogas slurry. Computational Fluid Dynamics (CFD) simulations were performed to validate the experimental results and provide deeper insights into the hydrocyclone's performance. This study is necessary because effective digestate management can enhance biogas plant sustainability. Recovered water can be reused within the system, reducing the need for freshwater, while solids can be developed into high-quality organic fertilizers. These outcomes promote resource efficiency, waste reduction, and the commercialization of sustainable biogas technologies. By addressing the challenges of digestate management, this study contributes to advancing biogas technology and supports global efforts toward sustainable waste management.

#### Design

The design of the current hydrocyclone is parametric, meaning that it is based on a principal dimension, specifically the body diameter (D). All other dimensions of the hydrocyclone are derived as ratios of this principal dimension. The essential design parameters are illustrated in Fig.. 1. The dimensional ratios for the design are listed in Table 1, and Table 2 provides the corresponding parameter values for a hydrocyclone with

a body diameter of 240 mm. These ratios were selected based on standard hydrocyclone design practices<sup>22,31</sup> to ensure optimal separation efficiency while maintaining ease of fabrication and operational stability. For instance:

The ratio H/D = 2.2083 determines the height-to-diameter proportion, ensuring sufficient residence time for particle separation.

The ratio  $\hat{D}_{e}/D = 0.2125$  governs the diameter of the vortex finder, controlling the overflow discharge and preventing particle bypass.

Other ratios, such as S/D and L./D, were chosen to balance the centrifugal force generation and flow stability.

These design considerations align with studies that emphasize the importance of dimensional ratios in optimizing hydrocyclone performance. For example, research has shown that adjusting parameters like vortex finder length and body height significantly impacts separation efficiency and operational performance<sup>9,31</sup>. Additionally, parametric optimization approaches have also been used to systematically refine hydrocyclone designs for enhanced separation, highlighting the critical role of these ratios in achieving desired outcomes<sup>22</sup>.

#### Experimental setup (Laboratory)

The hydrocyclone experiment is conducted in two stages. The initial setup is made in the Fluid Mechanics Laboratory of the Symbiosis Institute of Technology (SIT). The final installation is tested at the situ biogas plant on the SIT Campus. The initial setup consists of a hydrocyclone separator unit, a water tank, a submersible pump, a recirculatory overflow tank (ROT), and required pipe fitting. The water tank had a capacity of 1100 L, while the ROT could hold approximately 200 L. The submersible pump had a power rating of 3HP. The hydrocyclone separator was connected to the water tank through a pump that drew the charge (a mixture of water and sawdust) into the hydrocyclone inlet. The inlet was designed tangentially to the hydrocyclone walls to create a swirling flow inside the unit. This swirling motion generated two vortices, outer vortex (responsible for the underflow, where heavier particles were forced toward the hydrocyclone walls and collected in the collection chamber) and the inner vortex (responsible for the overflow, where lighter particles exited through the vortex finder).

A cutoff or bypass pipe was included in the setup to regulate flow rates. A control valve was installed above the pipe connecting the pump to the hydrocyclone inlet. This arrangement prevented excessive pressure gradients across the pump, which could exceed its working capacity and damage its operation. If the valve had been fitted below the inlet pipe, the pressure gradient would have increased to unsafe levels (Fig. 2). Fig. 3 illustrates this flow arrangement. The underflow charge was manually collected and weighed to calculate the collection efficiency, while the overflow charge was directed back to the ROT. The ROT's design ensured proper flow regulation:

At low flow rates, the tank did not fill to the upper outlet, and the charge exited through the lower outlet. At higher flow rates, the tank filled to the upper outlet, allowing the charge to exit through both the upper and lower outlets.

Flow rates were controlled using the flow control valve (FCV), and its angular position was carefully calibrated to approximate the desired flow rates. Table 3 lists the flow velocity and volumetric flow rates for different angular positions of the FCV. Fig. 2 shows a schematic of the laboratory setup, while Fig. 3 illustrates the actual experimental arrangement.

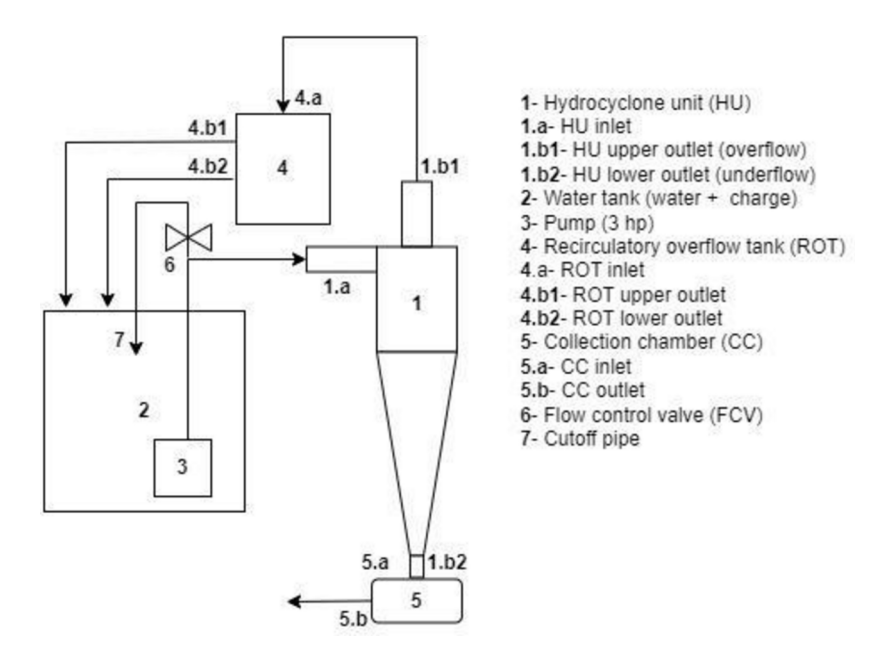


Fig.. 2. Schematic of the experimental setup.









**Fig.. 3**. Experimental setup in the Laboratory.

Sr. No	Flow rate (kg/s)	Volumetric flow rate (m3/s)	Flow Velocity (m/s)
1	1.57	0.00157	0.801
2	3.4	0.0034	1.727
3	5.09	0.00509	2.592
4	5.8	0.0058	2.949
5	6.044	0.006044	3.078

**Table 3**. Flow Velocity and Corresponding Volumetric Flow Rates for Different Angular Positions of the Flow Control Valve.

#### Experimentation, results, and discussion

Initially, a test run of 30 min was conducted to ensure satisfactory and stable operation of the equipment. The flow field stabilized approximately 15–20 min after starting the pump. Flow stability was evaluated by observing consistent particle trajectories, steady flow rates, and uniform separation performance over time. This duration ensured that the swirling motion inside the hydrocyclone reached a steady state, minimizing transient effects that could impact the separation efficiency. The flow stabilization period of 15–20 min was determined empirically by monitoring the uniformity of particle trajectories and the consistency of separation performance during preliminary tests. The turbulence losses observed at higher flow rates highlight the importance of operating within an optimal range to maintain effective separation. The study investigated the separation efficiency of a hydrocyclone using sawdust as the solute component. Five different flow rates were tested, with three readings taken for each flow rate to ensure accuracy and reliability. The effect of a coagulant (Ecoclean 20+) was also examined by adding it to the water tank in concentrations of 150 ppm and 200 ppm. The collection efficiency was calculated as the ratio of the weight of the collected underflow to the total weight of the solute mixed into the water. Results were plotted against the flow rate, as shown in Fig.. 4. Some key observations concerning the effect of the coagulant are discussed below (as mentioned in Table 4).

- 1. Without coagulant: The maximum collection efficiency was achieved at the lowest flow rate. As the flow rate increased, the efficiency decreased due to turbulence losses inside the hydrocyclone unit (HU). These turbulence losses refer to the excessive mixing and disruption of the flow caused by high velocities, which disturb the separation vortices. The outer and inner vortices, responsible for underflow and overflow, respectively, began to interact and destabilize at higher flow rates, reducing separation efficiency.
- With coagulant: The addition of the coagulant caused particles to settle prematurely, making it difficult for the pump to extract them. This led to a sharp decline in efficiency, even at low flow rates. The coagulant's

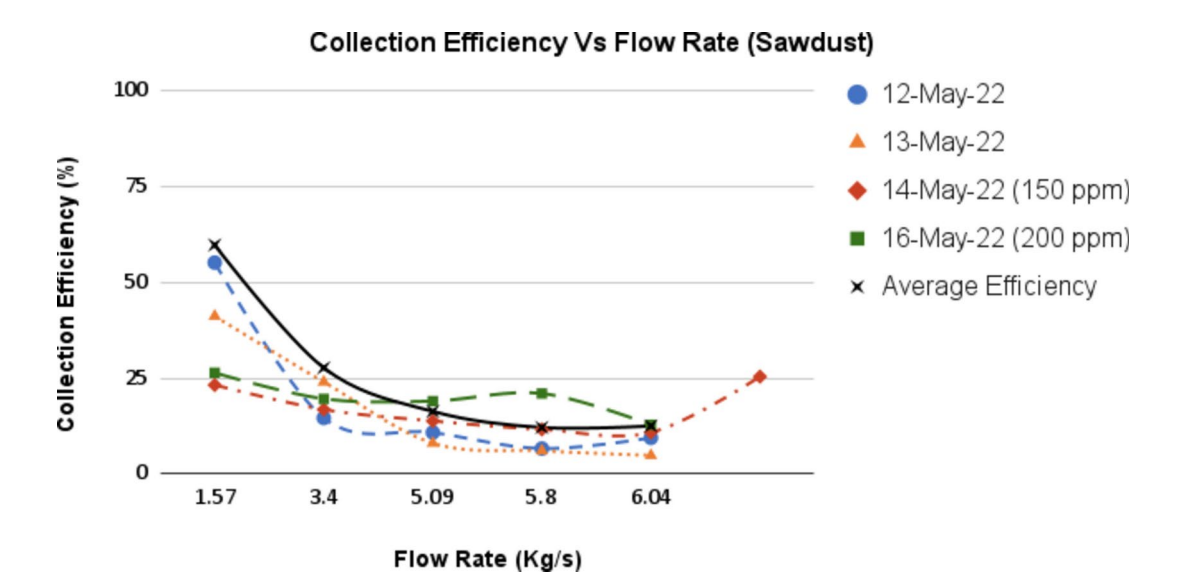


**Fig.. 4**. Flow rate Vs collection efficiency plot. Notice due to the effect of the coagulant, the collection efficiency declines.

Day-1	(12/05/22) – Wi	thout Coagulant				
Sr. No	Flow rate (kg/s)		Total weight mixed (kg)	Total weight collected (kg)	Collection efficiency (%	
1	1.57		5	3.38	67.6	
2	3.4		5	0.83	16.6	
3	5.09		5	0.64	12.8	
4	5.8		5	0.43	8.6	
5	6.04		5	0.57	11.4	
Day-2 (	(13/05/22) – Wit	thout Coagulant				
Sr. No	Flow rate (kg/s	s)	Total weight mixed (kg)	Total weight collected (kg)	Collection efficiency (%)	
1	1.57		5	2.06	41.2	
2	3.4		5	1.3	26	
3	5.09		5	0.5	10	
4	5.8		5	0.4	8	
5	6.04		5	0.34	6.8	
Day-3 (	(14/05/22) – Wi	th Coagulant (150	PPM)			
Sr. No	Sr. No Flow rate (k		Total weight mixed (kg) Total weight collected (kg)		Collection efficiency (%)	
1		1.57	5	1.16	23.2	
2	3.4		5	0.94	18.8	
3	3 5.09		5	0.79	15.8	
4	5.8		5	0.68	13.6	
5		6.04	5	0.64	12.8	
Day-4 (	(16/05/22) – Wit	th Coagulant (200	PPM)			
Sr. No		Flow rate (kg/s)	Total weight mixed (kg)	Total weight collected (kg)	Collection efficiency (%)	
1	1.57		5	1.32	26.4	
2	3.4		5	0.98	19.6	
3 5.09		5	0.95	19		
4 5.8		5	1.05	21		
5 6.04		5	0.64	12.8		

**Table 4**. Experimental Data on Collection Efficiency for Different Flow Rates with and without Coagulant Additions.

effect on particle settling reduced the effectiveness of the swirling flow, which relies on suspended particles for optimal separation.

The results demonstrate that the hydrocyclone performs best at lower flow rates without the addition of coagulants. Excessive flow rates and the use of coagulants negatively impact separation efficiency due to turbulence and particle settling, respectively. Proper control of flow rates and solute properties is critical for optimizing hydrocyclone performance.

#### Experimental setup (In-situ biogas plant)

After completing the laboratory tests, the hydrocyclone setup was installed and tested at the biogas plant on the Symbiosis Institute of Technology (SIT) Fig.. 5 campus (Fig.. 6). The in-situ setup retained most components from the laboratory setup, with two key modifications: the recirculatory overflow tank (ROT) was excluded and two additional stages were added: a preprocessing unit (PU) and the biomass/biogas plant (BMP). Numerous studies have demonstrated the use of hydrocyclones in anaerobic digesters to enhance biogas plant performance and separate various particulates, such as organic matter, plastics, and fine sand, from wastewater<sup>10–13</sup>. The present study focuses on sludge/slurry dewatering and recirculation, and researchers have previously numerically and experimentally examined sludge dewatering<sup>14–16</sup>. The present study uses a conventional design for the hydrocyclone, although hydrocyclones with numerous structural developments have been tested numerically and experimentally<sup>17</sup>. Researchers have also optimized existing designs for more efficient and enhanced separation<sup>18</sup>. A few new designs have also been proposed for the separation of numerous different particulates and finer particles, such as plastics and oil, from wastewater<sup>19–22</sup>. The schematic of the modified setup is shown in Fig.. 5. The biogas waste reservoir (BWR) contained the waste product from the BMP, which included biogas slurry. A pump placed inside the BWR drew the slurry and directed it to the hydrocyclone unit (HU) inlet. The slurry entered the HU tangentially, creating a swirl-dominated flow that generated two vortices<sup>32</sup>.

Outer vortex: Directed heavier particles toward the HU walls, where they were collected in the collection chamber (CC) and discharged through the underflow outlet.

Inner vortex: Carried lighter particles to the overflow outlet, which directed the material back to the BWR.

The underflow material collected in the CC was further processed into manure or similar products, benefiting the institute and nearby farmers. The overflow material, consisting primarily of water, was recirculated back into the BMP to reduce the need for freshwater. This recirculation introduced beneficial microorganisms into the pre-digestion chamber, enhancing biogas production. The biogas slurry separation experiment was conducted over multiple iterations. The residues from the overflow and underflow were collected for 15 s to evaluate the hydrocyclone's separation efficiency (Table 5). The separation efficiency was calculated as the ratio of the collected underflow material to the total slurry fed into the HU. Results indicated that the overflow contained significantly less slurry than the underflow, demonstrating effective separation of water from dense slurries. The separated water, constituting 24–40% of the total slurry volume, was reused in the biogas plant. This reduced the demand for fresh water and enhanced the sustainability of the biogas production process. Similar studies have also highlighted the importance of hydrocyclone design and operating parameters, such as feed velocity, pressure, and particle characteristics, in optimizing separation efficiency<sup>20,22–24</sup>.

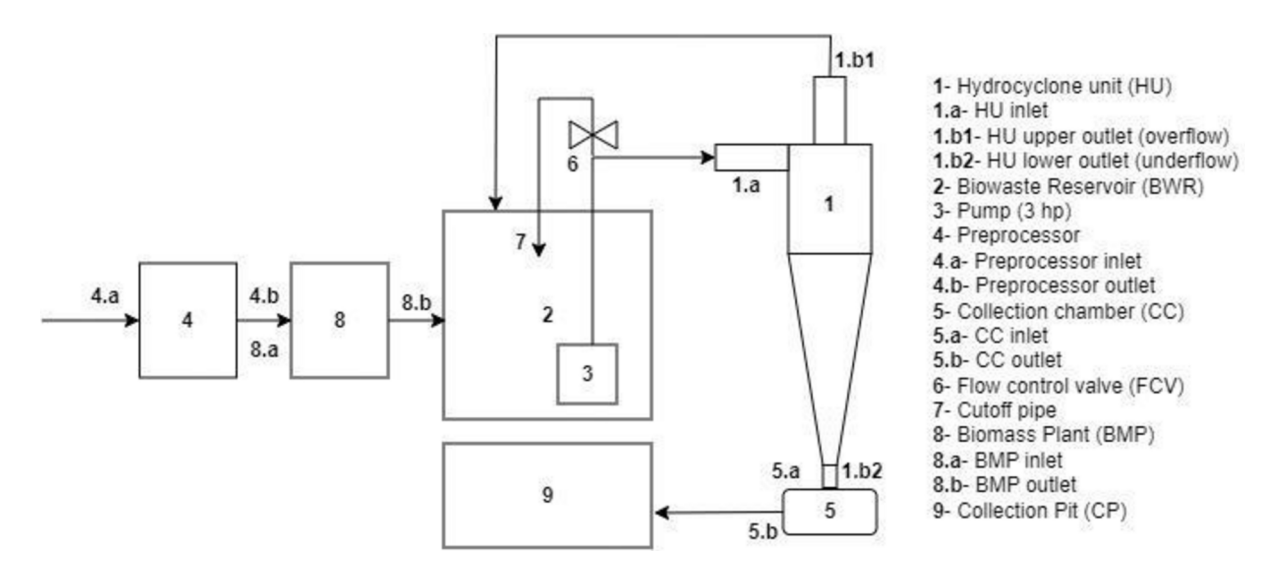


Fig. 5. Schematic of the BMP setup.



Fig.. 6. (a) BMP, (b) Experimental setup, (c) BWR, (d) Dried slurry collected at CP.

Sr. No	Flow rate (kg/s)	Total Residues (Kg)	Residues without Water (kg)	Underflow (Kg)	Overflow (Kg)	Efficiency (%)
1	1.57	23.55	4.71	3.46	1.05	73.46
2	3.4	51	10.2	8.07	1.52	79.11
3	5.09	76.35	15.27	12.61	1.84	82.58
4	5.8	87	17.4	12.52	2.42	71.95
5	6.044	90.6	18.12	13.84	2.47	76.37

Table 5. Residues collected for 15 s.

# **Numerical analysis**

General description

A Numerical analysis of the flow domain was also performed using Computational Fluid Dynamics (CFD) on the Fluent module of ANSYS. The 3D Navier–Stokes equations were solved using an unstructured grid. The Navier–Stokes equations were spatially discretized using a second-order accurate upwind finite-volume scheme. The Euler fluxes were discretized by a Coupled pressure–velocity coupling scheme, which basically refers to the numerical approach used to solve the governing equations. In this scheme, the pressure and velocity fields are solved simultaneously, rather than sequentially, ensuring better convergence and stability for complex flow domains. This method is particularly effective for swirling flows, where strong interactions between pressure and velocity gradients occur.Because the geometry of the flow domain is complex to solve in the transient stage, a pseudo-time method is applied to the formulation. The renormalized Groups (RNG) k– $\epsilon$  model with a swirl-dominated flow method and standard wall functions is used for the solution of the flow domain.

Since the early work of Jones and Launder<sup>25</sup>, the k- $\epsilon$  model has been used to examine recirculating as well as swirl flows. The RNG  $k-\epsilon$  model is an advanced version of the standard turbulent model. The RNG  $k-\epsilon$  model was derived by Kenneth using a rigorous statistical<sup>26-28</sup>. This model is similar to the standard model but comes with a few refinements, such as it is able to handle swirling and rotating flows with higher accuracy, and provides an analytical formulation for the turbulent Prandtl number which ensures consistency in the transport properties of the turbulence model. It is also suitable for low-Reynolds-number flows; therefore, the RNG k- $\epsilon$  model is more reliable and accurate than its predecessor.

The transport equations for the RNG k-ε model are,

$$\frac{\partial}{\partial t}(\rho k) + \frac{\partial}{\partial x_i}(\rho k u_i) = \frac{\partial}{\partial x_j} \left(\alpha_k \mu_{eff} \frac{\partial k}{\partial x_j}\right) + G_k + G_b - \rho \varepsilon + Y_M + S_k \tag{1}$$

and

$$\frac{\partial}{\partial t}(\rho\varepsilon) + \frac{\partial}{\partial x_i}(\rho\varepsilon u_i) = \frac{\partial}{\partial x_j}\left(\alpha_\varepsilon\mu_{eff}\frac{\partial\varepsilon}{\partial x_j}\right) + C_{1\varepsilon}\frac{\varepsilon}{k}\left(G_k + G_{3\varepsilon}G_b\right) - C_{2\varepsilon}\frac{\varepsilon^2}{k} - R_\varepsilon + S_\varepsilon \tag{2}$$

Here,  $G_k$  represents the generation of turbulence kinetic energy owing to mean velocity gradients.  $G_b$  is the generation of turbulence kinetic energy owing to buoyancy. The quantities  $\alpha_k$  and  $\alpha_\varepsilon$  are the inverse effective Prandtl numbers of k and  $\varepsilon$ , respectively.  $S_k$  and  $S_\varepsilon$  are user-defined source terms.

The RNG model in Fluent provides an option to account for the effects of swirl or rotation by appropriately modifying turbulent viscosity. The functional form of this modification is as follows:

$$\mu_t = \mu_{t0} f\left(\alpha_s, \Omega, \frac{k}{\varepsilon}\right) \tag{3}$$

where  $\mu_{t0}$  is the turbulent viscosity calculated without swirl modification.  $\Omega$  is a characteristic swirl number that is evaluated by the fluent itself, and swirl modification takes place for rotating and three-dimensional flows.  $\alpha_s$  is the swirl constant and assumes different values depending on whether the flow is highly or mildly swirl-dominated. For highly swirl-dominated flows (strong rotational motion with minimal axial disturbance), its value was set to 0.07, although for strongly swirl-dominated flows (significant axial flow disturbances), higher values may be used. Davailles et al.<sup>19</sup> conducted a detailed swirling flow pattern, and a physics-based model that describes the swirl-dominated flow was established, numerically simulated by the semi-industrial code NEPTUNE CFD, and validated from existing experimental results.

The inverse effective Prandtl numbers for the k and  $\epsilon$  equations are derived analytically using RNG theory and are given as follows:

$$\left| \frac{\alpha - 1.3929}{\alpha_0 - 1.3929} \right|^{0.6321} \left| \frac{\alpha + 2.3929}{\alpha_0 + 2.3929} \right|^{0.3679} = \frac{\mu_{mol}}{\mu_{eff}}$$
 (4)

where  $\alpha_0 = 1.0$ 

The main difference between the standard and RNG models is that the addition term of  $R_{\varepsilon}$  in the equation is given by

$$R_{\varepsilon} = \frac{C_{\mu}\rho\eta^{3} \left(1 - \frac{\eta}{\eta_{0}}\right)}{1 + \beta\eta^{3}} \frac{\varepsilon^{2}}{k} \tag{5}$$

where  $\eta \equiv \frac{Sk}{\varepsilon}$  ,  $\eta_0 = 4.38, \beta = 0.012$ 

Using Eq. 5, Eq. 2 can be rewritten as

$$\frac{\partial}{\partial t}(\rho\varepsilon) + \frac{\partial}{\partial x_i}(\rho\varepsilon u_i) = \frac{\partial}{\partial x_j} \left(\alpha_\varepsilon \mu_{eff} \frac{\partial \varepsilon}{\partial x_j}\right) + C_{1\varepsilon} \frac{\varepsilon}{k} \left(G_k + G_{3\varepsilon}G_b\right) - C_{2\varepsilon}^* \rho \frac{\varepsilon^2}{k}$$
 (6)

where  $C_{2\varepsilon}^*$  is given as:

$$C_{2\varepsilon}^* = C_{2\varepsilon} + \frac{C_{\mu}\rho\eta^3 \left(1 - \frac{\eta}{\eta_0}\right)}{1 + \beta\eta^3} \tag{7}$$

In regions where  $\eta < \eta_0$  or the strain rate is comparatively less, R gives positive contributions and  $C_{\varepsilon\varepsilon}^2$  increases; for the regions of large strain rates, the converse is true. Near the log layer,  $\eta \approx 3.0$ , giving  $C_{\varepsilon\varepsilon}^2 \approx 2.0$ , which is very close to the value of  $C_{2\varepsilon}$  in the standard model. Consequently, for swirling or rotating flows, the RNG model is more relevant to the effects of rapid staining.

The model constant are given as follows:

$$C_{1\varepsilon} = 1.42, C_{2\varepsilon} = 1.68, C_{\mu} = 0.0845, \alpha_s = 0.07$$
 (8)

The particle force balance equation can be used to write the equations for the discrete phase model (DPM) for tracking the paths of particles as<sup>29</sup>

$$\frac{du_i^p}{dt} = F_p \left( u_i - u_i^p \right) + \frac{g_i(\rho_p - \rho)}{\rho_p} + \frac{F_i}{\rho_p} \tag{9}$$

where

$$\begin{split} F_p\left(u_i-u_i^p\right) &= \text{drag force function of the relative velocity.} \\ \frac{g_i(\rho_p-\rho)}{\rho_p} &= \text{force of gravity.} \\ \frac{F_i}{\rho_p} &= \text{forces depending on the flow conditions (additional forces).} \end{split}$$

#### Results and discussion

The Fluent setup described earlier was used to simulate the hydrocyclone separator. The RNG  $k-\epsilon$  turbulence model was employed to simulate the incompressible turbulent multiphase flow. A second-order accurate upwind finite volume approach was used to spatially discretize the Navier–Stokes equations, and the Euler fluxes were discretized using a coupled pressure–velocity scheme. The pseudo-time method was applied to simplify the transient formulation, allowing for efficient computation of the complex swirling flow. The multiphase flow was managed using the Volume of Fluid (VOF) formulation<sup>30</sup>, and suspended particles were tracked using the Discrete Phase Model (DPM). Fig. 7a shows the hydrocyclone separator while Fig.. 7b, c,d presents the outer mesh along with the mesh sections. The hydrocyclone was meshed using ICEM CFD, and a mesh convergence study was conducted with three different meshes:

- 1. Coarse Mesh: 16,858 nodes, 83,373 mixed elements.
- 2. Medium Mesh: 24,573 nodes, 123,174 mixed elements.
- 3. Fine Mesh: 48,626 nodes, 249,119 mixed elements.

The medium mesh was selected for all simulations based on the mesh independence study. Fig. 8 illustrates the pressure and velocity changes along the hydrocyclone axis for various mesh sizes. Here, there is a significant overlap between the medium and fine meshes, and there is also a 3.2% error between the two, compared with a 5.6% difference between the coarse and medium meshes. Consequently, a medium mesh was used for all calculations. Mesh refinement was systematically performed in regions of high gradients, such as near the walls and vortex zones, to capture critical flow features accurately. Contours for different meshes are also presented in Fig. 9. Boundary layer meshes were created adjacent to cyclone walls to resolve velocity gradients near the wall accurately. The computational cell size was approximately 2.5—5 mm near the wall and 10–15 mm in the core regions. While this cell size is larger than the average particle diameter (10 mm), the DPM tracing assumption was validated by ensuring that the mesh resolution was sufficient to resolve the particle trajectories and capture particle—wall interactions accurately.

The suspended particles adhere to a no-slip boundary at the hydrocyclone walls and exhibit a "reflective" behavior upon impact. This assumption is valid because of the diverse nature of the incoming fluid, which comprises air, suspended solids, and water. When the particles collide with the cyclone wall, they rebound as per the "reflective" boundary condition. The outlet at the hydrocyclone base, which was open to atmospheric pressure, employed a far-field pressure condition. The inlet velocities (90-370 lpm) that correspond to the required flow rate are given as the velocity inlet boundary conditions for the cross-section. All three species of air, water, and suspended particles that stand in for sawdust are considered to have the same intake velocity. The volume percentage and size of the suspended particles were controlled using discrete phase model injection inputs. We attempted to reproduce our experimental results by separating solid suspended sawdust particles using CFD. The average particle size, density, and velocity were considered in sufficient detail to accurately depict the motion of suspended solid particles. The movement of particles was assumed to follow a uniform distribution. These suspended particles mirror the suspended solid particles in the manure and have an average particle diameter of 10 mm and an average density of 210 kg/m3. Their sizes ranged from 1 to 100 mm in diameter. We injected approximately 2050 suspended particles using the spray injection function from the intake as per the Rosin–Rammler distribution<sup>29</sup>. The residuals for all the flow variables ultimately converged to less than 10-6 levels to achieve a steady solution during each CFD simulation. Convergence was assessed not only by observing residuals but also by monitoring physical parameters such as velocity, pressure, and particle trajectories at key locations within the hydrocyclone. This ensured that the solution was physically meaningful and consistent with experimental observations.

For an input flow velocity of 0.801 m/s, Fig. 10 depicts the pressure contours, tangential velocity at the midplane, monitored particle trajectory, and velocity streamlines. Fig. 10a clearly shows that the pressure drops around the cylindrical region were the highest and gradually decreased along the conical section. The centrifugal force causes heavy particles to be pushed downward and towards the cyclone wall. Fig. 10b demonstrates that the tangential velocity increased along the radial direction, indicating that the centrifugal forces were active in the cyclone's radial direction. The tangential velocity generated inside the cyclone can be used to estimate the magnitude of the developed tangential forces. Particle track traces for an inlet velocity of 0.801 m/s are shown in Fig.. 10c. Solid suspended particles move in cyclonic motion and are collected or separated from the cyclone's lower outlet. The cyclones or swirling motions produced inside the cyclone are shown in Fig.. 10d from where it is possible to detect two vortices forming counterclockwise.

Fig. 11 compares the hydrocyclone's collection efficiency for various flow rates. The efficiency increased with flow rates from 1.57 to 5.09 kg/s, but a steep decline was observed at 5.7 kg/s due to disruption of the inner and outer vortices owing to over-mixing. These losses disrupted the separation vortices, reducing the hydrocyclone's effectiveness. At flow rates above 6 kg/s, the efficiency increased again, likely due to improved

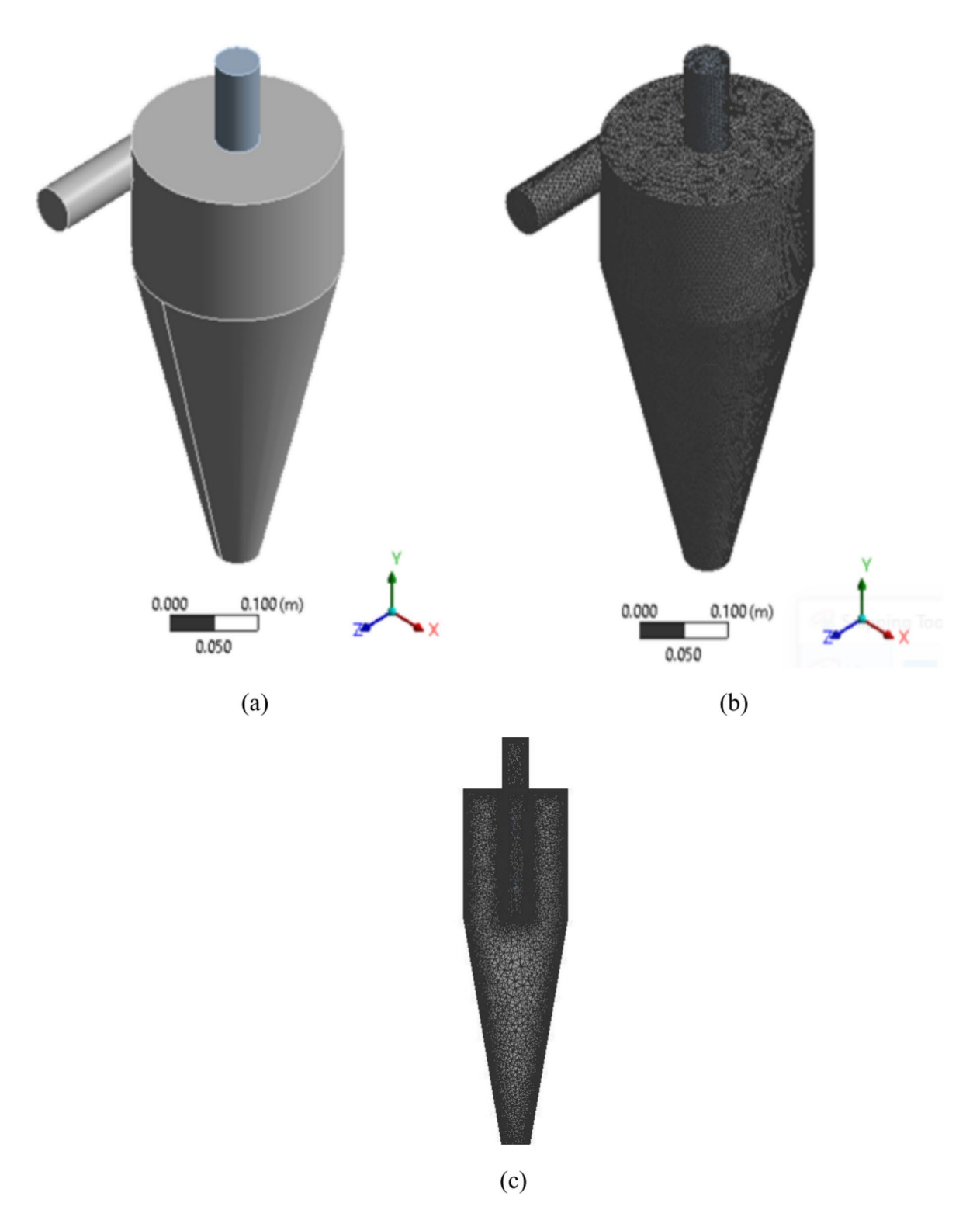


Fig.. 7. (a) 3D geometry of the separator, (b) Meshed fluid domain, (c) and (d) illustrates the sections of the meshed separator section.

particle entrainment at higher velocities. Frictional losses in the piping system are neglected for the numerical simulation leading to very high collection efficiency. The ideal flow rate range was determined to be 3–5 kg/s based on both experimental and simulation results. The sudden decline in the collection efficiency predicted by the CFD simulation in comparison to the experiment around 5.07 kg/s may be due to the ineffectiveness of the turbulence model used. RNG k –  $\epsilon$  turbulence model, while effective for capturing swirling flows, may not fully account for the complex interactions at high flow rates, especially near the vortex finder or in regions with strong



Figure 7. (continued)

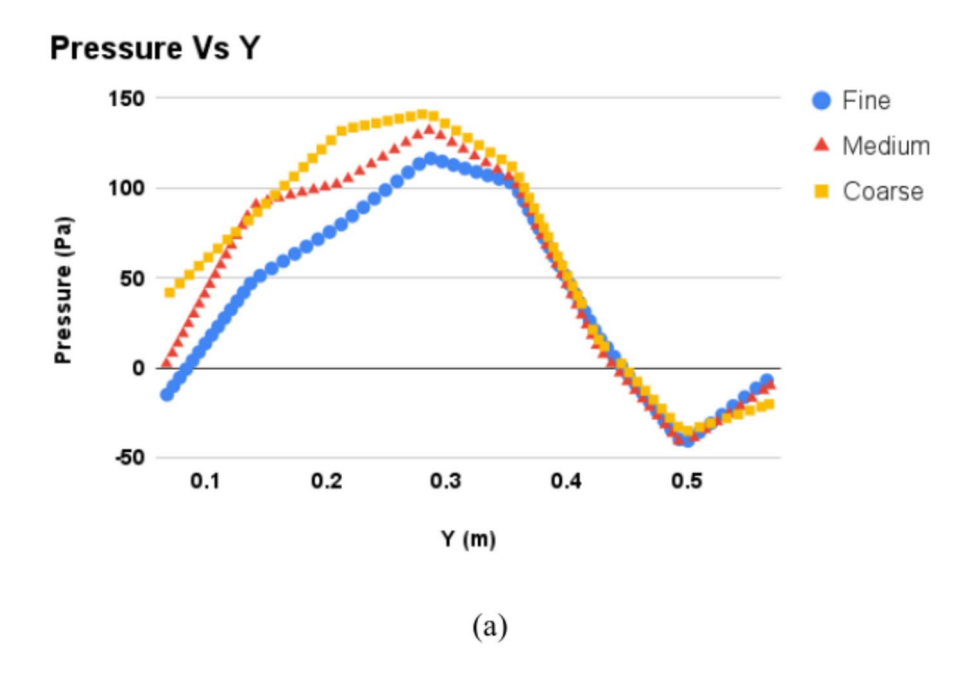
shear layers. The DPM also only accounts for the drag and centrifugal forces and doesn't take into account the particle–particle, particle wall interactions (collisions).

The numerical simulations of the hydrocyclone separator provided valuable insights into its performance and flow dynamics. The mesh convergence study established that the medium mesh (24,573 nodes and 123,174 mixed elements) offered an optimal balance between computational efficiency and accuracy, with less than a 3.2% error compared to the fine mesh. The systematic refinement of critical regions, such as near the walls and vortex zones, ensured accurate resolution of velocity gradients and particle-wall interactions. Boundary layer meshes were employed to resolve near-wall velocity gradients accurately, correcting the earlier misstatement that they enforce the no-slip condition. The computational cell size was validated as appropriate for Discrete Phase Model (DPM) tracing, ensuring that particle trajectories and interactions were adequately captured. The simulations revealed key flow features, including high static pressure near the cylindrical region, strong tangential velocities indicating effective centrifugal forces, and well-defined cyclonic particle trajectories. However, at higher flow rates (around 5.7 kg/s), excessive mixing disrupted the separation vortices, leading to a sharp decline in collection efficiency. Beyond 6 kg/s, efficiency improved due to better particle entrainment, but this flow regime is less stable. The collection efficiency was consistent with experimental results, with the ideal flow rate range identified as 3-5 kg/s. This range balances turbulence-induced losses and particle separation efficiency. Convergence criteria were enhanced by monitoring physical parameters, such as velocity and pressure, in addition to residuals, ensuring that the simulations were both numerically and physically accurate. Despite the overall effectiveness of the hydrocyclone, limitations were observed, the turbulence model requires further refinement to capture near-wall effects accurately. A detailed y + study should be conducted in future simulations to ensure mesh suitability near the wall. The simulations demonstrated the hydrocyclone's ability to separate solid particles effectively under optimized conditions, while also highlighting areas for improvement. Future work should explore advanced turbulence models, refine mesh generation strategies, and investigate the effects of varying particle properties and flow conditions to enhance predictive accuracy and operational performance.

#### Conclusion

This study investigated the performance of a hydrocyclone separator for solid-liquid separation in a biogas plant setting through experimental and numerical approaches. The research demonstrated the potential of the hydrocyclone to enhance resource efficiency by separating suspended solids from biogas slurry, reclaiming water for reuse, and producing nutrient-rich solids for agricultural applications. In the experimental phase, both laboratory and in-situ biogas plant setups were tested. Laboratory experiments revealed that the hydrocyclone achieved a maximum collection efficiency of approximately 67% at lower flow rates without the use of coagulants. The addition of coagulants adversely affected separation efficiency due to premature particle settling, highlighting the need for optimized coagulant usage. In the biogas plant setup, the hydrocyclone effectively reclaimed 24–40% of the water content from the biogas slurry, reducing the demand for fresh water and enhancing sustainability. However, approximately 30–40% of suspended particles remained in the reclaimed water, indicating room for improvement in separation performance. The numerical analysis provided deeper insights into the flow dynamics within the hydrocyclone. The simulations accurately captured critical flow features, including pressure contours, tangential velocities, and particle trajectories. The RNG  $k-\epsilon$  turbulence model, combined with refined meshing, effectively simulated swirling flows and particle separation. The mesh convergence study validated the medium mesh as optimal, with a systematic refinement approach ensuring accuracy in critical regions.

Despite the promising results, several areas for improvement and limitations have been identified:



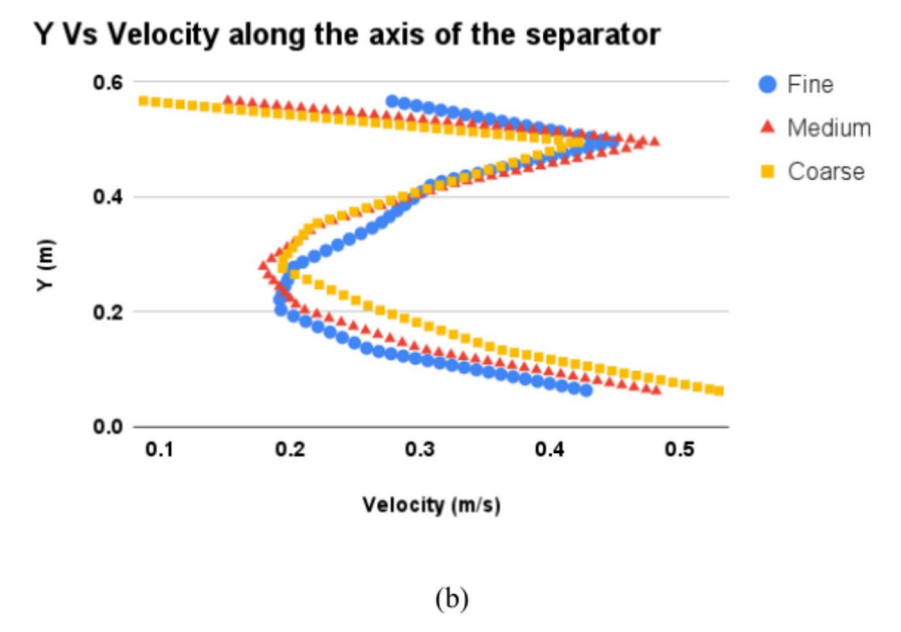
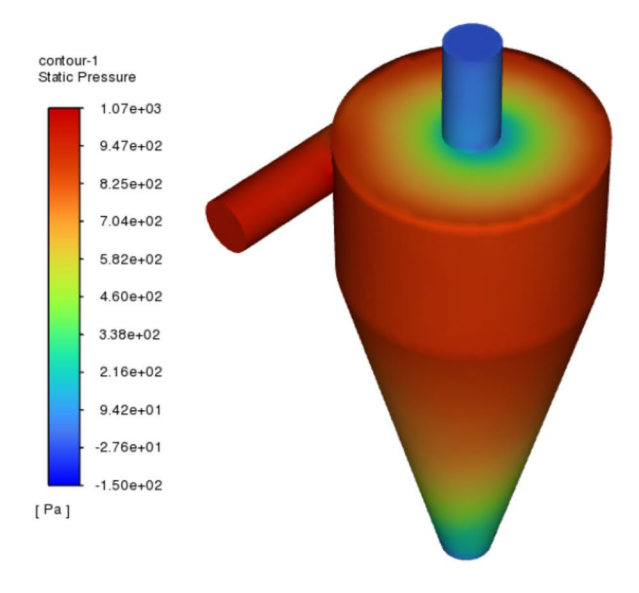


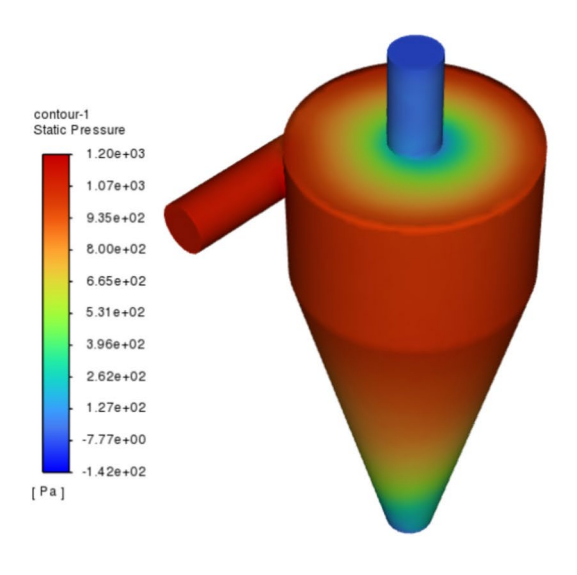
**Fig.. 8**. Results along the axis for different mesh a. Pressure b. Velocity. Notice the significant overlap between the medium and fine meshes for both velocity as well as pressure plots.

- 1. Turbulence Modeling: The RNG  $k-\epsilon$  model showed good performance but requires further refinement to capture near-wall effects. Incorporation of a detailed y+study in future work would enhance precision.
- 2. Mesh Suitability: The mesh convergence study was adequate enough to ensure that the accuracy is reasonable, but there is still room for optimization of particle and cell sizes to further enhance the accuracy of DPM tracing assumptions.
- 3. Operational Limits: It was found that at higher flow rates, the efficiency of the hydrocyclone reduces due to losses in turbulence. Advanced designs or multi-stage hydrocyclones may be able to overcome this problem.
- 4. Coagulant Optimization: The usage of coagulants has to be further optimized to achieve an optimal balance between particle settling and separation efficiency.

This research underscores the significant role hydrocyclones can play in boosting the sustainability of biogas plants by enabling water reclamation and generating valuable by-products. The findings successfully bridge the gap between experimental observations and numerical predictions, laying a solid foundation for optimizing hydrocyclone performance. Moving forward, future studies should delve into advanced turbulence models, refined meshing techniques, and the use of multi-stage hydrocyclones to further enhance separation efficiency.



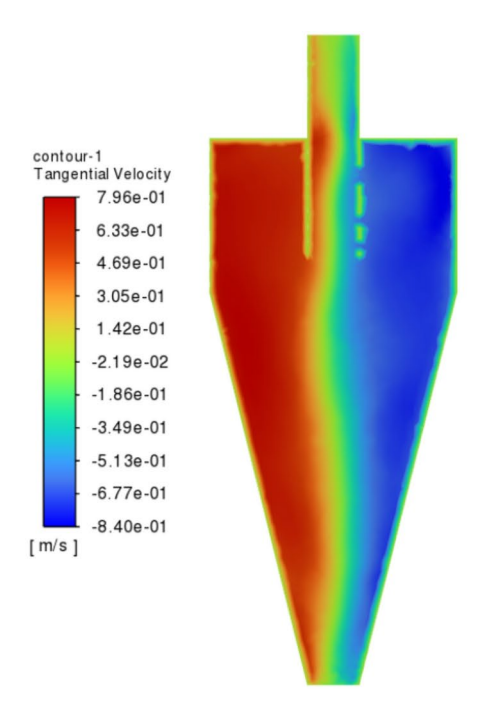
# (a) Static Pressure contour for medium mesh at inlet velocity of 0.81 m/s



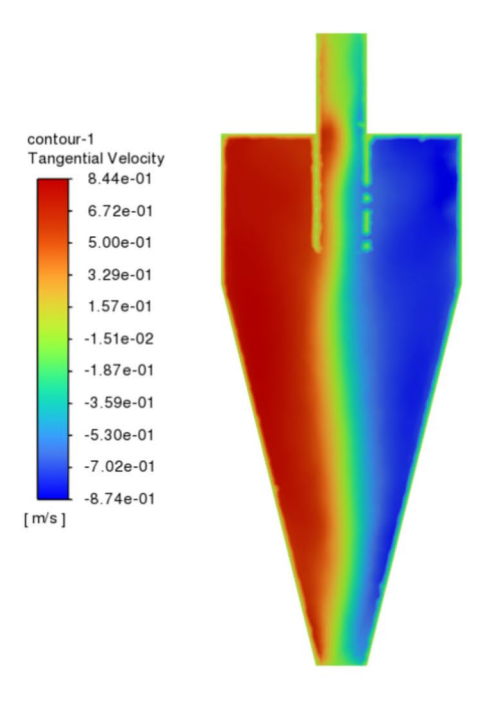
# (b) Static Pressure contour for fine mesh at inlet velocity of 0.81 m/s

Fig. 9. Static pressure (a, b) and tangential velocity (c, d) contours are illustrated for medium and fine meshes respectively. Notice the minimal change in the flow variables and the flow field.

Investigating the impact of coagulants and particle characteristics under varying flow conditions could also provide valuable insights for operational improvements. Addressing these challenges will allow hydrocyclone technology to be more effectively tailored to the specific needs of biogas plants, ultimately advancing sustainable waste management and resource recovery efforts.

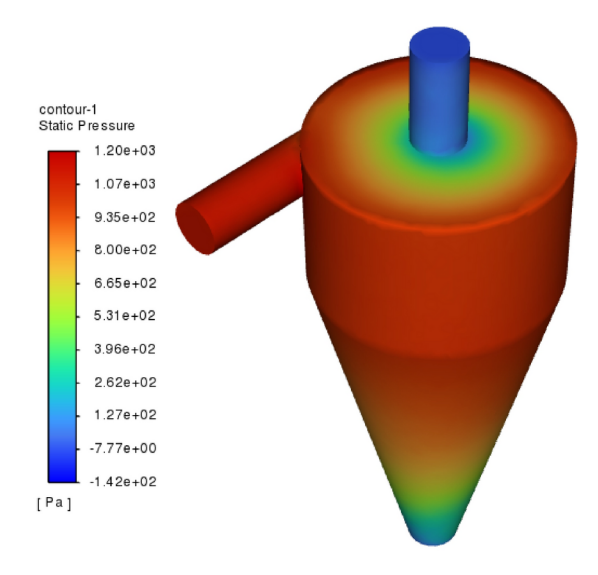


(c) Tangential velocity contour for medium mesh at inlet velocity of 0.81 m/s

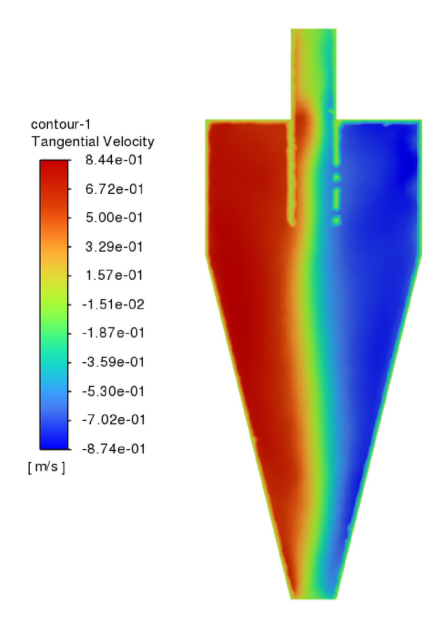


(d) Tangential velocity contour for fine mesh at inlet velocity of 0.81 m/s

Figure 9. (continued)



(a) Pressure contours show the highest static pressure near the cylindrical region, gradually decreasing along the frustum section. This pressure drop generates the centrifugal forces responsible for particle separation.



(b) Tangential velocity contours indicate increasing velocity along the radial direction, confirming strong centrifugal forces.

**Fig.. 10**. Different contours (for inlet velocity 0.81 m/s): (a) Static pressure, (b) Tangential velocity, (c) Particle tracks- Particle trajectories reveal cyclonic motion, with heavier particles collected at the underflow and lighter particles exiting through the overflow, (d) Velocity streamlines- Swirling flow patterns highlight the interaction between the inner and outer vortices, both rotating counterclockwise.

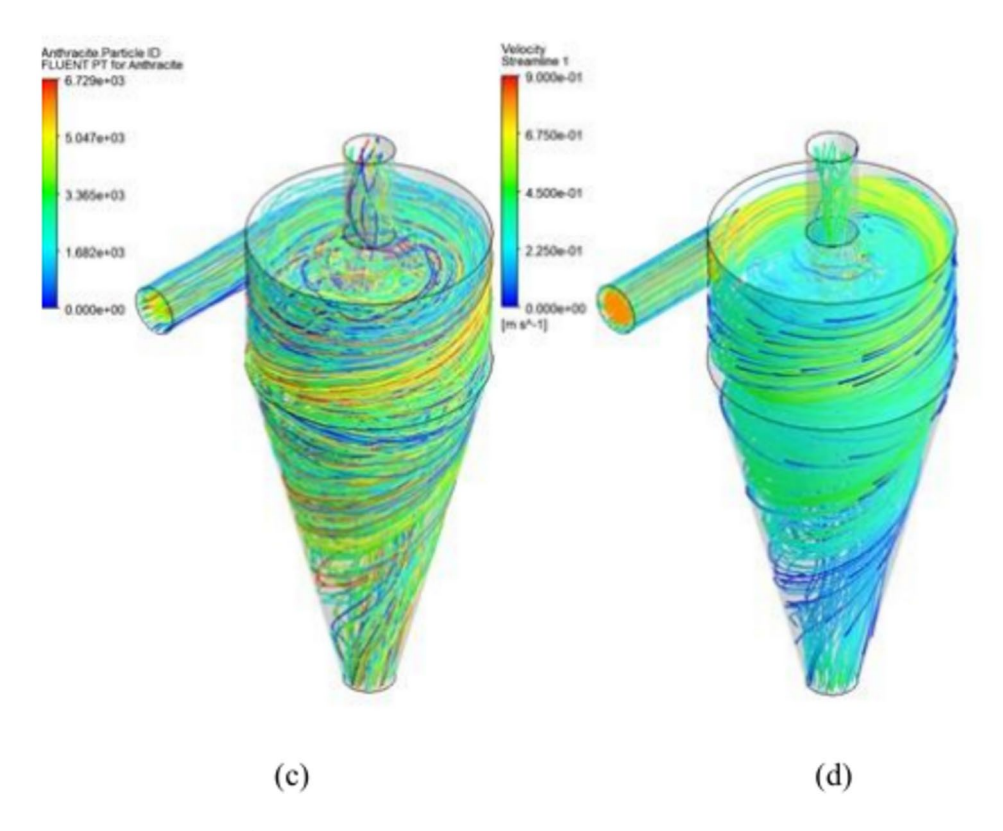


Figure 10. (continued)

# Collection Efficiency Vs Flow Rate

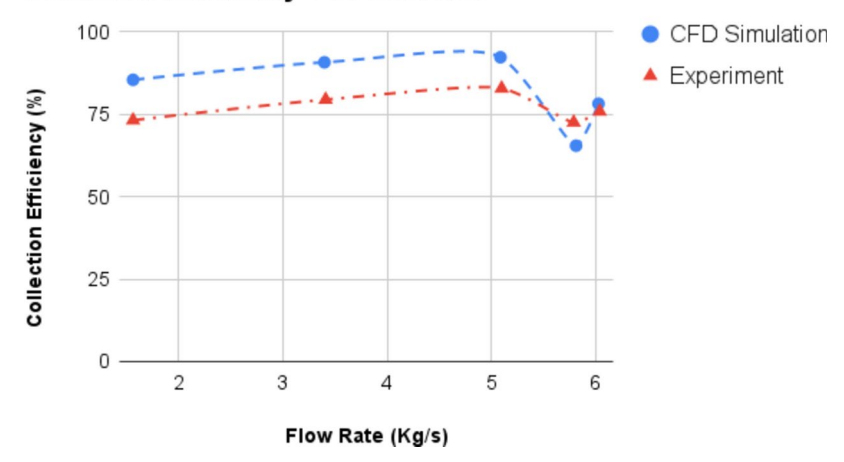


Fig.. 11. Flow rate Vs collection efficiency plot. The collection efficiency predicted by the CFD simulation suddenly declines as the RNG  $k-\epsilon$  turbulence model, while effective for capturing swirling flows, may not fully account for the complex interactions at high flow rates, especially near the vortex finder or in regions with strong shear layers.

#### Data availability

Data will be available by sending reasonable request to the Corresponding author.

Received: 15 December 2024; Accepted: 19 February 2025

Published online: 07 March 2025

# References

1. Breitenmoser, L. et al. Anaerobic digestion of biowastes in India: Opportunities, challenges and research needs. *J. Environ. Manage.* 236, 396–412. https://doi.org/10.1016/j.jenvman.2018.12.014 (2019).

- 2. Popovic, O., Gioelli, F., Dinuccio, E., Rollè, L. & Balsari, P. Centrifugation of digestate: The effect of chitosan on separation efficiency. Sustain. 9, 1–9. https://doi.org/10.3390/su9122302 (2017).
- 3. Kumar, S. et al. Challenges and opportunities associated with waste management in India. R. Soc. Open Sci. 4, 160764. https://doi.org/10.1098/rsos.160764 (2017).
- Mirmohamadsadeghi, S., Karimi, K., Tabatabaei, M. & Aghbashlo, M. Biogas production from food wastes: A review on recent developments and future perspectives. Bioresour. Technol. Bioeng. 7, 100202. https://doi.org/10.1016/j.biteb.2019.100202 (2019).
- 5. Al-Wahaibi, A. et al. Techno-economic evaluation of biogas production from food waste via anaerobic digestion. Sci. Rep. 10, 72897. https://doi.org/10.1038/s41598-020-72897-5 (2020).
- Bao, Y., Fu, Y., Wang, C. & Wang, H. An effective integrated system used in separating for anaerobic digestate and concentrating for biogas slurry. Environ. Technol. (United Kingdom) 42, 4434

  –4443. https://doi.org/10.1080/09593330.2020.1761457 (2021).
- Mudryk, K., Fraczek, J., Jewiarz, M., Wróbel, M. & Dziedzic, K. Analysis of mechanical dewatering of digestate. Agric. Eng. 20, 157–166. https://doi.org/10.1515/agriceng-2016-0073 (2016).
- Schwinghammer, L., Krause, S. & Schaum, C. Determination of large microplastics: Wet-sieving of dewatered digested sludge, cosubstrates, and compost. Water Sci. Technol. 84, 384–392. https://doi.org/10.2166/wst.2020.582 (2021).
- Jank, A. et al. Hydrocyclones for the separation of impurities in pretreated biowaste. Waste Manag. 64, 12–19. https://doi.org/10.1 016/j.wasman.2017.03.001 (2017).
- 10. Bayo, J., López-Castellanos, J., Martínez-García, R., Alcolea, A. & Lardín, C. Hydrocyclone as a cleaning device for anaerobic sludge digesters in a wastewater treatment plant. J. Clean. Prod. 87, 550–557. https://doi.org/10.1016/j.jclepro.2014.10.064 (2015).
- 11. Sun, Y. et al. Hydrocyclone-induced pretreatment for sludge solubilization to enhance anaerobic digestion. *Chem. Eng. J.* **374**, 1364–1372. https://doi.org/10.1016/j.cej.2019.05.159 (2019).
- 12. Huang, X., Lu, Y., Wu, G. & Liu, Z. Research on the experiment of the enhancement removal of fine sand by hydrocyclone in sewage treatment plant. *Environ. Sci. Pollut. Res.* 28, 337–353. https://doi.org/10.1007/s11356-020-10493-w (2021).
- de Laclos, H. F., Desbois, S. & Saint-Joly, C. Anaerobic digestion of municipal solid organic waste: Valorga full-scale plant in Tilburg, the Netherlands. Water Sci. Technol. 36, 457–462. https://doi.org/10.1016/S0273-1223(97)00555-6 (1997).
- Liu, Y. et al. Sludge disintegration using a hydrocyclone to improve biological nutrient removal and reduce excess sludge. Sep. Purif. Technol. 177, 192–199. https://doi.org/10.1016/j.seppur.2016.11.001 (2017).
- Yang, I. H., Shin, C. B., Kim, T. H. & Kim, S. A three-dimensional simulation of a hydrocyclone for the sludge separation in water purifying plants and comparison with experimental data. *Miner. Eng.* 17, 637–641. https://doi.org/10.1016/j.mineng.2003.12.010 (2004).
- Rizk, S. A., Mageed, A. A. & Abu-Ali, M. H. Dewatering the sludge generated from water treatment plants with two hydrocylones in series. J. Eng. Sci. 38, 797–806 (2010). https://doi.org/10.21608/jesaun.2010.124399.
- 17. Yuan, Y., et al. Structural improvement of the cyclone separator for separating the biogas impurity particles. *Energy Sources Part A Recover. Util. Environ. Eff.* 00, 1–14 (2020). https://doi.org/10.1080/15567036.2020.1815905.
- 18. Ni, L. et al. Optimizing geometric parameters in hydrocyclones for enhanced separations: A review and perspective. Sep. Purif. Rev. 48, 30–51. https://doi.org/10.1080/15422119.2017.1421558 (2019).
- 19. Li, F. et al. Purification of granular sediments from wastewater using a novel hydrocyclone. *Powder Technol.* **393**, 751–763. https://doi.org/10.1016/j.powtec.2021.08.025 (2021).
- Rocha, C. A. O., Ullmann, G., Silva, D. O. & Vieira, L. G. M. Effect of changes in the feed duct on hydrocyclone performance. *Powder Technol.* 374, 283–289. https://doi.org/10.1016/j.powtec.2020.07.001 (2020).
- Senfter, T., et al. Field study on the removal of solid impurities in wastewater treatment plants by implementing a modified hydrocyclone. Int. Conf. Transp. Sediment. Solid Particles TS 19, 293–300 (2019).
- 22. Tian, J., Ni, L., Song, T., Olson, J. & Zhao, J. An overview of operating parameters and conditions in hydrocyclones for enhanced separations. Sep. Purif. Technol. 206, 268–285. https://doi.org/10.1016/j.seppur.2018.06.015 (2018).
- 23. Chu, L. Y., Chen, W. M. & Lee, X. Z. Effects of geometric and operating parameters and feed characters on the motion of solid particles in hydrocyclones. Sep. Purif. Technol. 26, 237–246. https://doi.org/10.1016/S1383-5866(01)00171-X (2002).
- 24. Braun, T. & Bohnet, M. Influence of feed solids concentration on the performance of hydrocyclones. *Chem. Eng. Technol.* 13, 15–20. https://doi.org/10.1002/ceat.270130104 (1990).
- 25. Jones, W. P. & Launder, B. E. The prediction of laminarization with a two-equation model of turbulence. *Int. J. Heat Mass Transf.* 5, 413–418 (1992).
- 26. Launder, B. E. & Sharma, B. I. Application of the energy-dissipation model of turbulence to the calculation of flow near a spinning disc. Lett. Heat Mass Transf. 1, 131–137. https://doi.org/10.1016/0094-4548(74)90150-7 (1974).
- Yakhot, V., Orszag, S. A., Thangam, S., Gatski, T. B. & Speziale, C. G. Development of turbulence models for shear flows by a double expansion technique. *Phys. Fluids A* 4, 1510–1520. https://doi.org/10.1063/1.858424 (1992).
- 28. Wilson, K. G. The renormalization group and critical phenomena. *Rev. Mod. Phys.* 55, 583–600. https://doi.org/10.1103/RevMod Phys.55.583 (1983).
- Sawant, R. V. & Sonawane, C. R. Numerical simulations of bore-finishing tool lubrication system to achieve minimum quantity lubrication using the discretized phase model. *Lect. Notes Mech. Eng.* 767–778 (2019). https://doi.org/10.1007/978-981-13-6469-3
- 30. Sonawane, C. R. et al. Numerical simulation of hydro-cyclone separator used for separation of highly dense suspended particulate matter. *Mater. Today: Proc.* **59**, 85–92. https://doi.org/10.1016/j.matpr.2021.10.208 (2022).
- 31. Yuan, Y., Zhao, Z., Tan, L., Xu, Y. & Yuan, Y. Structural improvement of the cyclone separator for separating biogas impurity particles. Energy Sources Part A Recover. Util. Environ. Eff. (2020). https://doi.org/10.1080/15567036.2020.1815905.
- 32. Gupta, R. et al. Studies on the understanding mechanism of air core and vortex formation in a hydrocyclone. Chem. Eng. J. 144, 153–166. https://doi.org/10.1016/j.cej.2008.01.010 (2008).

# **Acknowledgements**

The authors extend their appreciation to the fund support provided by Symbiosis International (Deemed University), Pune India through Minor research funding (SIU/ SCRI/MRP/2020/1497). The authors also extend their appreciation to the Researchers Supporting Project number (RSPD2025R999), King Saud University, Riyadh, Saudi Arabia.

# **Author contributions**

Ishan Mishra, Rohan Sawant, and Manikprabhu Dhanorkar were responsible for conceptualization, software development, visualization, and writing. Kamal Sharma and Chandrakant Sonawane contributed to software development. Md. Irfanual Haque Siddiqui, Ghanshya Tejani, and Intesaaf Ashraf oversaw project administration and secured funding for the project.

# **Funding**

Open access funding provided by Symbiosis International (Deemed University).

#### **Declarations**

### Competing interests

The authors declare no competing interests.

### Additional information

Correspondence and requests for materials should be addressed to C.S.

Reprints and permissions information is available at www.nature.com/reprints.

**Publisher's note** Springer Nature remains neutral with regard to jurisdictional claims in published maps and institutional affiliations.

Open Access This article is licensed under a Creative Commons Attribution-NonCommercial-NoDerivatives 4.0 International License, which permits any non-commercial use, sharing, distribution and reproduction in any medium or format, as long as you give appropriate credit to the original author(s) and the source, provide a link to the Creative Commons licence, and indicate if you modified the licensed material. You do not have permission under this licence to share adapted material derived from this article or parts of it. The images or other third party material in this article are included in the article's Creative Commons licence, unless indicated otherwise in a credit line to the material. If material is not included in the article's Creative Commons licence and your intended use is not permitted by statutory regulation or exceeds the permitted use, you will need to obtain permission directly from the copyright holder. To view a copy of this licence, visit <a href="http://creativecommons.org/licenses/by-nc-nd/4.0/">http://creativecommons.org/licenses/by-nc-nd/4.0/</a>.

© The Author(s) 2025